Journal of Materials Chemistry C

Nanotube array-based barium titanate-cobalt ferrite composite film for affordable magnetoelectric multiferroics

Journal:	*Journal of Materials Chemistry C*
Manuscript ID	TC-ART-05-2019-002442.R1
Article Type:	Paper
Date Submitted by the Author:	22-Jul-2019
Complete List of Authors:	Kawamura, Go; Toyohashi University of Technology, Oura, Kentaro; Toyohashi University of Technology Tan, Wai Kian; Toyohashi University of Technology Goto, Taichi; Toyohashi University of Technology Nakamura, Yuichi; Toyohashi University of Technology Yokoe, Daisaku ; Japan Fine Ceramic Center Francis, Leonard; International Iberian Nanotechnology Laboratory, Hajraoui, Khalil; International Iberian Nanotechnology Laboratory Wei, xing; 1School of Materials Science and Engineering, Chang'an University Inoue, Mitsuteru; Toyohashi University of Technology Muto, Hiroyuki; Toyohashi University of Technology, Electrical - Electronics Information Engeneering Yamaguchi, Kazuhiro; National Institute o Technology Ibaraki College, Electrical and Electronic Engineering course Boccaccini, Aldo; Univ. of Erlangen-Nuremberg, Matsuda, Atsunori; Toyohashi University of Technology, Electrical and Electronic Information Engineering

ARTICLE

Nanotube array-based barium titanate-cobalt ferrite composite film for affordable magnetoelectric multiferroics

Received 00th January 20xx,
Accepted 00th January 20xx

DOI: 10.1039/x0xx00000x

Go Kawamura,*[ab] Kentaro Oura,[a] Wai Kian Tan,[c] Taichi Goto,[ad] Yuichi Nakamura,[a] Daisaku Yokoe,[e] Francis Leonard Deepak,[f] Khalil El Hajraoui,[f] Xing Wei,[g] Mitsuteru Inoue,[a] Hiroyuki Muto,[c] Kazuhiro Yamaguchi,[h] Aldo R. Boccaccini[b] and Atsunori Matsuda[a]

Magnetoelectric multiferroic nanocomposites are increasingly attracting attention from researchers and engineers due to their transformative technological potential. Many papers have so far reported the fundamental understandings, designs of new multiferroic nanocomposites, and their potential applications. However, many challenges for establishing and expanding their applications remain, for example, the development of an affordable fabrication process for nanocomposites which show room temperature multiferroics with robust coupling between ferroelectricity and magnetism is one of the highest demands. In this work, an affordable liquid phase based method to fabricate a magnetoelectric multiferroic nanocomposite film is reported. Ferroelectric $BaTiO_3$ (BTO) nanotube arrays are fabricated via anodization and hydrothermal treatment, and then spin-coated with ferrimagnetic $CoFe_2O_4$ (CFO) to obtain BTO-CFO nanocomposite film. The film exhibits not only room-temperature multiferroicity but also perpendicular magnetic anisotropy.

Introduction

Multiferroic materials that show magnetoelectric effect have been attracting much attention because of their potential applications in novel memories, transducers, actuators, and microwave reactors.[1-3] Because single-phase materials showing multiferroicity at room temperature are rare,[4] two-phase materials composed of ferro/ferrimagnetics and ferroelectrics with various composite structures have been widely investigated over the last 50 years.[5-9] The coupling between different ferroic orders in such two-phase composites arises from strain transfer at the phase boundaries,[10] thus an interface design/engineering is important to maximize the strain transfer.

Traditional sol-gel processes using metal alkoxides or metal salts as the starting materials were occasionally employed to fabricate two-phase composites, for example, with mono-, bi- and multi-layer structures.[11-13] However, since proactive interface engineering as well as protecting the formation of side phases and cracks was difficult in such simple sol-gel processes, relatively weak magnetoelectric effects were reported.

On the other hand, mixtures of two kinds of ferroic nanoparticles have been prepared by various processes including electrospinning,[14] solid-state reactions,[15] and also sol-gel methods.[16,17] Such nanoparticle-based magnetoelectric nanocomposites can have a large interfacial area where the strain transfer occurs. Erdem et al. prepared a $BaTiO_3$-$CoFe_2O_4$ (BTO-CFO) nanoparticle-based nanocomposite thin film with a co-dispersed composite geometry via a sol-gel spin coating process.[17] The components were well dispersed at nanoparticle level in the nanocomposite film, securing the formation of a large interfacial area. As a result of efficient strain transfer between the two components, room-temperature electric control of magnetism was experimentally confirmed though it was categorized as a coupling of ferroelectric and superparamagnetic orders, which is not multiferroics. With the co-dispersed composite geometry, the interfacial area can be increased by decreasing the size of nanoparticle components. However, small nanoparticles do not exhibit ferro/ferrimagnetism but superparamagnetism due to random flip of magnetization under the influence of temperature. Therefore, a large magnetoelectric effect cannot be expected.

Gas phase syntheses were found to provide multiferroic nanocomposite films with a relatively large magnetoelectric

[a]Department of Electrical and Electronic Information Engineering, Toyohashi University of Technology, 1-1 Hibarigaoka, Tempaku-cho, Toyohashi, 441-8580 Aichi, Japan. E-mail: gokawamura@ee.tut.ac.jp
[b]Institute of Biomaterials, University of Erlangen-Nuremberg, Germany
[c]Institute of Liberal Arts and Science, Toyohashi University of Technology, Japan
[d]JST, PRESTO, Japan
[e]Nanostructures Research Laboratory, Japan Fine Ceramics Center, Japan
[f]Nanostructured Materials Group, Department of Advanced Electron Microscopy, Image and Spectroscopy, International Iberian Nanotechnology Laboratory, Portugal
[g]School of Materials Science and Engineering, Chang'an University, China
[h]Electrical and Electronic Engineering Course, National Institute of Technology, Ibaraki College, Japan

† Electronic Supplementary Information (ESI) available: SEM images, STEM-EDX analyses, COMSOL simulations, a photo of magnetoelectric effect measurement setup, and table listing magnetic properties. See DOI: 10.1039/x0xx00000x

effect.[18] Among various microstructures of the films, Zheng et al. first reported the clear advantages of the vertically aligned magnetic nanopillars embedded in an electric matrix, in which the energy of elastic interactions among two components could become very large due to the large interfacial area and the weak substrate clamping effect.[19] Followed by their pioneering research, nanocomposites with similar nanopillar array-based structures have attracted attention, and their favorable properties, such as large magnetoelectric effect and anisotropic magnetization, for various practical applications, have been reported by several researchers.[2,20-22] However, the complex growth processes resulted in the difficulty in achieving the right crystallinity and stoichiometry of the phases, and also the extraordinarily high manufacturing costs.[23]

Among various selections of electric and magnetic components, BTO and CFO are recognized as one of the best combinations to achieve strong magnetoelectric coupling via stress mediation.[2,24] This is because of not only their individual piezoelectric and magnetostrictive properties but also their possible structural compatibility which even allows the formation of an epitaxial interface.[2,19]

In this regard, we have recently fabricated BTO-CFO multiferroic nanocomposites with nano-periodic structures using a sol-gel templating method, which can avoid high manufacturing costs.[25,26] In this method, an anodic aluminum oxide template was used to obtain, for example, ferrimagnetic CFO nanotube arrays, then the arrays were embedded in a ferroelectric BTO matrix. This structure resembles the nanopillar array-based nanomaterial prepared via gas phase processes, thus the same advantages can be expected, namely, strong magnetoelectric effect due to the large interfacial area and weak substrate clamping effect. Although a clear magnetoelectric effect was not detected, the multiferroicity of our nanocomposite films was confirmed. For obtaining better multiferroic properties including a room temperature magnetoelectric effect and anisotropic magnetization, a more precise control of the nanostructure is necessary.

The important novelty in this work is an affordable and simple fabrication proce**ss for a** multiferroic BTO-CFO nanocomposite film, which shows a magnetoelectric effect and anisotropic magnetization at room temperature. Briefly, highly ordered and vertically oriented TiO_2 nanotube arrays (TNTs) were formed on a Ti substrate by anodization. The TNTs and a $Ba(OH)_2$ aqueous solution were put in a pressure vessel for subsequent hydrothermal treatment to convert TiO_2 to BTO without collapsing the nanotubular structure of TNTs.[27,28] The obtained BTO nanotube arrays (BTO NTs) were then spin-coated with a CFO precursor solution to form a BTO-CFO multiferroic nanocomposite film. The structure of the nanocomposite was thoroughly investigated and was correlated with the magnetic, dielectric, and magnetoelectric properties.

Results and discussion

The SEM images of typical anodization-derived TNTs before and after hydrothermal treatment in a $Ba(OH)_2$ aqueous solution are shown in **Figs. 1A**, **1B**, **1C** and **1D**. The caliber and the length of the TNTs were ~100 and ~2500 nm (see Figs. 1A and 1B), respectively. The dimensions of the TNTs changed by the hydrothermal treatment to be 40-50 nm for the caliber and ~2600 nm for the length (see Figs. 1C and 1D). The dimension alteration is presumably a result of the following reaction occurring during the hydrothermal treatment,[27,28] leading to a thickening of the walls of the nanotube arrays.

$$Ba(OH)_2 + TiO_2 \rightarrow BaTiO_3 + H_2O$$

It is noteworthy that the nanotube array structure did not collapse despite the large volume increase of the sample during the hydrothermal treatment. In this work, the experimental conditions for anodization and hydrothermal treatment were carefully selected in order to maintain the nanotube array structure of the sample. In other words, there were an optimum temperature and concentration of the $Ba(OH)_2$ aqueous solution for the hydrothermal treatment for each TNT dimension. In fact, the nanotube array structure was not maintained when the TNT walls were too thin, and unreacted TiO_2 remained when the walls were too thick or the concentration of $Ba(OH)_2$ was lower than 0.04 M.

The formation of BTO was also confirmed by X-ray diffraction (XRD) measurements (**Fig. 2**). Since there was no peak except for the peaks from the Ti substrate (JCPDS: 44-1294) in the XRD pattern of TNTs, the amorphous state of TiO_2 before hydrothermal treatment was confirmed. On the other hand, the sample after hydrothermal treatment exhibited peaks of perovskite BTO (JCPDS: 05-0626) in addition to the Ti peaks. The complete conversion of TiO_2 to BTO was roughly confirmed by the observation of no TiO_2-related peaks from the XRD pattern of the sample which was heated at 600 °C for 3 hrs in air after hydrothermal treatment. The energy-dispersive X-ray spectroscopy (EDX) measurements further proved that almost all TiO_2 was converted to BTO because the atomic ratio of Ba:Ti was approximately 1:1 (**Table S1**), whereas the

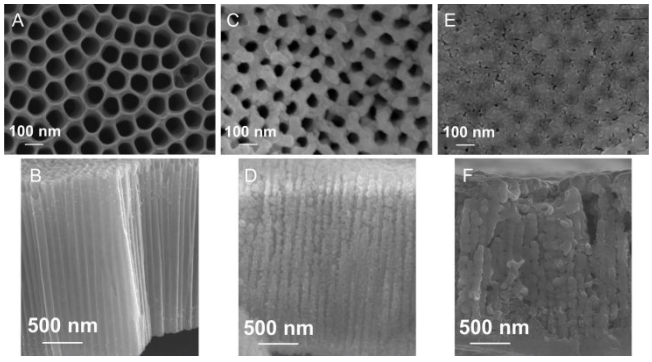

Fig. 1 SEM images of TNTs (A, B), BTO NTs (C, D), and BTO-CFO nanocomposite films.

ratio was about 1:2 at the bottom region of the nanotube arrays; this is probably due to the signal from the Ti substrate.

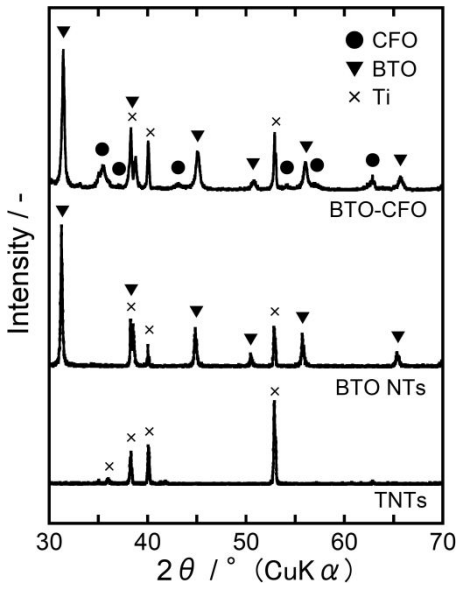

Fig. 2 XRD patterns of TNTs, BTO NTs, and BTO-CFO nanocomposite film.

The BTO nanotube arrays were then spin-coated 10 times with a freshly prepared CFO precursor solution. Compared with the SEM images of the BTO nanotube arrays (Figs. 1C and 1D), the surface SEM image of the sample after the spin coating process showed that the pores of the BTO nanotube arrays were closed (**Fig. 1E**), and the cross-sectional image revealed that the walls of the BTO were thickened (**Fig. 1F**). The observed morphology changes would be explained by the following two phenomena occurring during the 10 time CFO spin coating process: 1. Initially, the exposed surface including the inner walls of the BTO nanotube arrays was homogeneously coated with CFO; 2. At the end of the process (about at the 10th coating), the tube top is preferentially coated with CFO because of the narrowed tubular pores which would not allow the CFO solution to penetrate deep into the nanotubes. These assumptions were experimentally confirmed by changing the cycle numbers of coating. As the coating number was increasing, the caliber of the tubular pores was narrowing step by step, but after the 10th coating process a pure CFO layer formed on the top of the nanotube arrays instead of filling the tubular pores completely (see **Fig. S1**). Therefore, the spin coating process was repeated only 10 times in this work in order to avoid the formation of a pure CFO layer on the top of the BTO-CFO nanocomposite film.

The XRD pattern of the BTO-CFO nanocomposite film showed spinel CFO peaks (JCPDS: 22-1086) in addition to perovskite BTO and substrate Ti peaks (Fig. 2). It is noteworthy here that there was no unexpected XRD peaks from the nanocomposite film even though a heat treatment at 600 °C for 3 hrs was performed after the spin coating of BTO NTs with the CFO precursor solution. This confirmed that there was no significant distribution of the elements between BTO and CFO, meaning that a clear interface of BTO and CFO formed, which would result in an efficient strain transfer between BTO and CFO.

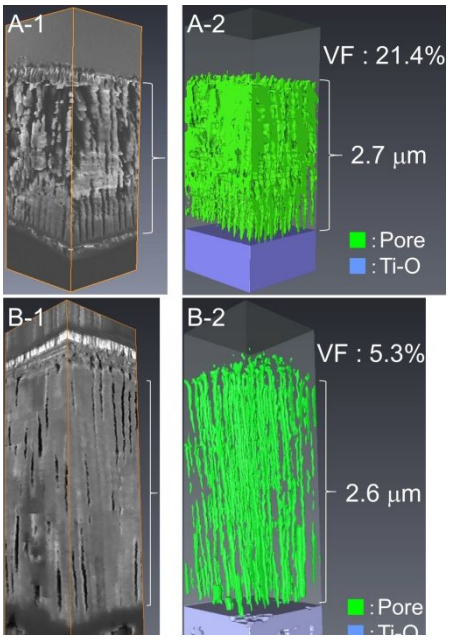

Fig. 3 3-dimensional SEM image (-1) and void mapping (-2) of BTO NTs (A) and BTO-CFO nanocomposite film (B).

The BTO-CFO nanocomposite film was obtained as a result of spin coating of BTO NTs with CFO. However, it seemed that there was still a certain amount of void in the nanocomposite film, judging from the SEM images shown in Fig. 1. Therefore, the void structures in the samples were carefully investigated using a 3-dimensional SEM technique. Before coating with CFO, the BTO NTs had tubular voids with a void fraction of 21.4% (**Figs. 3A-1** and **3A-2**). The tubular voids were apparently narrowed by CFO coating accompanied with a reduction of the void fraction to 5.3% (**Figs. 3B-1** and **3B-2**), confirming that 16.1% (in volume fraction) of the nanocomposite film was composed of CFO. The narrowed tubular voids observed in the images also indicated that the inner walls of BTO NTs were coated with CFO. Thus the elemental distribution of Ti and Fe was then recorded to investigate the distribution of BTO and CFO in the nanocomposite film. The tubular voids of the nanocomposite film were clearly seen in the high angle annular dark field-scanning transmission electron microscope (HAADF-STEM) image and the corresponding elemental mapping created from the energy-dispersive X-ray spectroscopy (EDX) data (**Fig. 4**), meaning that a sufficient spatial resolution of measurement was assured. In addition, Ti (pink in color) and Fe (blue in color) were detected from the same positions, meaning no segregation of the elements of Ti and Fe was seen in the mapping image. This also indicated that the BTO NT inner walls were homogeneously coated with CFO, proving that the nanocomposite film possessed a large interfacial area between BTO and CFO. Further analyses especially on the crystalline orientations etc. using STEM-EDX technique were carried out, and the results are shown in **Fig. S2**.

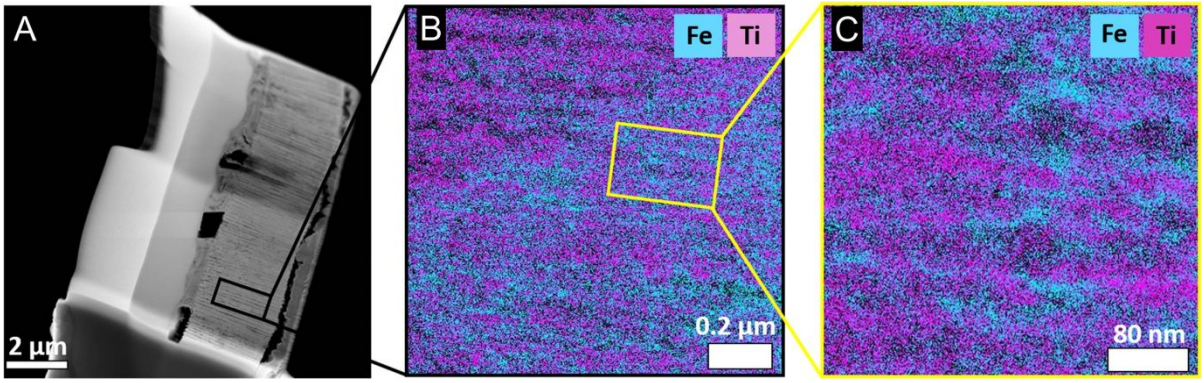

Fig. 4 HAADF-STEM image of a lamella extracted from the BTO-CFO nanocomposite film (A). EDX mappings on the area defined by the black (B) and yellow (C) boxes showing the distribution of Fe and Ti elements along the tubular channels.

Nanocomposites composed of vertically aligned ferrimagnetic square nanopillars embedded in a ferroelectric matrix had theoretically and experimentally proved to possess advantages for magnetoelectric effect due to the large interfacial area and the weak substrate clamping effect.[2,18] We fabricated a similar structure, but not the same one, thus computer simulations were first carried out to confirm whether or not the present nanocomposite film had similar advantages in terms of magnetoelectric effect. As a result of the simulation, our nanotube array-based composite film showed superiority in comparison to conventional bilayer and multilayer composite films in terms of strain transfer, which is a key phenomenon for the magnetoelectric effect. The detailed conditions and interpretations of the computer simulation are shown in **Fig. S3**.

An experimental approach to the magnetoelectric effect of the BTO-CFO nanocomposite film was carried out by recording its dielectric hysteresis loops with and without applying an external magnetic field (**Fig. 5**). The shape of the loops showed an obvious change when a bias field of 3.5 kG was applied to the film, meaning that our nanocomposite film exhibited a room temperature magnetoelectric effect. The saturation polarization values, P_0 and P_{350}, were 197 to 393 nC cm^{-2}, respectively, and the proportion, $(P_{350}-P_0)/P_0\times100$, was 99%, which was much higher than those in previous reports.[29-32] This is presumably because of the unique nanotube array-based structure, which has two important advantages for the magnetoelectric effect, as mentioned above. On the other hand, judging from the recorded hysteresis loops, the leakage current seemed to be fairly large. With respect to this issue, heat treatment of the nanocomposite at higher temperature, as well as optimizing the porous structure of the nanocomposite film,[33-35] would be further necessary for reducing leakage. Regarding the heat treatment at higher temperature, our preliminary trial failed because of the reactions of the Ti substrate with an atmosphere containing oxygen and nitrogen, resulting in the fracture of the substrate at temperatures higher than 700 °C. A substrate exchange process for TNTs would therefore be needed for improving dielectric property by high temperature heat treatment, and this is one of our future challenges.[36]

The magnetic properties of pure CFO and BTO-CFO nanocomposite films were measured at room temperature using both in plane and out of plane configurations (**Fig. 6**). The coercivity and remnant magnetization values of each film are summarized in **Table S2**; the values of the two films were similar to those reported by other groups.[37,38] On the other hand, shape anisotropy of magnetization is expected in our nanocomposite film due to the anisotropic nanotube array-based structure; while others such as crystalline and surface anisotropies can be neglected because the film is polycrystalline, and its thickness is not in the range of angstroms.[39] The easy axis for magnetization in the pure CFO film was apparently in the in-plane direction, where the magnetic field was applied parallel to the substrate. This is a general result because of the shape anisotropy of the thin film. On the other hand, the magnetization in the BTO-CFO nanocomposite film was slightly easier when the magnetic field was applied in the out-of-plane direction compared to the magnetization with an in-plane configuration. In general, a nanowire array-like ferro/ferrimagnetic material fabricated using a nanotube array template possesses an easy magnetization axis in the out-of-plane direction (perpendicular magnetic anisotropy).[40] Therefore, even though our nanocomposite film contained narrow tubular pores with a volume fraction of 5.3%

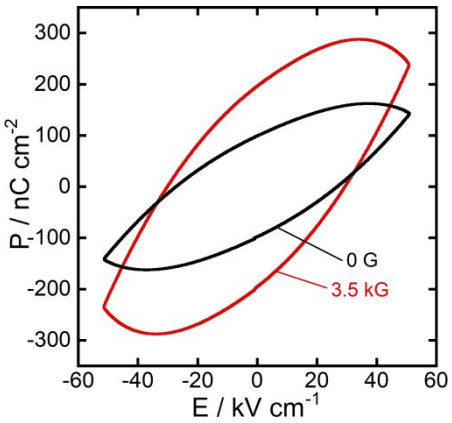

Fig. 5 Dielectric hysteresis loops of BTO-CFO nanocomposite film with and without applying an external magnetic field. The measurement frequency was 100 Hz.

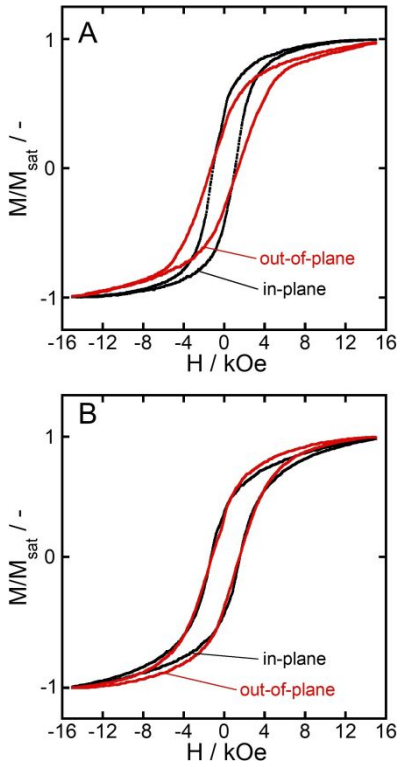

Fig. 6 Magnetic hysteresis loops of pure CFO (A) and BTO-CFO nanocomposite films (B). The magnetization values were normalized to the corresponding saturation magnetization values.

and the walls of BTO NTs were not smooth like previous reports,[41] it exhibited perpendicular magnetic anisotropy. This is an important advancement in the multiferroic research field because multiferroic nanocomposite films with perpendicular magnetic anisotropy, which opens up new fields of application such as functionalized arrays of magnetic sensors and patterned magnetic recording media,[40,41] have never been previously fabricated using only affordable liquid phase processes.

Experimental

TNTs were prepared by a two-step anodization process. For the first step, a Ti foil (15×20×0.2 mm^3; Nilaco Co., Japan) was anodized in an ethylene glycol-based electrolyte containing 0.09 M NH_4F and 1.24 M H_2O at 60 V, 20 °C for 2 hrs. The formed un-uniform TNTs were then completely removed by ultrasonication of them in H_2O in order to obtain a macroscopically even surface of the Ti foil with periodic nanovoids. The second anodization was carried out to the Ti foil using a masking tape with a pore diameter of 12 mm. The electrolyte used was a mixture of ethylene glycol and dimethyl sulfoxide (molar ratio; 1 : 1) containing 0.1 M NH_4F and 1.5 M H_2O, and the conditions of the second anodization were 60 V, 60 °C, and 1 min. After 1 min of anodization, the foil was kept in the electrolyte for 15 min under stirring to remove carbon-rich phase from the TNT surface.

The obtained uniform TNTs were immersed into a 0.1 M $Ba(OH)_2$ aqueous solution and were heated and kept at 180 °C for 2 hrs in a Teflon lined hydrothermal reactor to convert TiO_2 to BTO without collapsing the nanotube array structure.

For the preparation of CFO precursor solution, 0.05 M $Co(CH_3COO)_2{\cdot}4H_2O$ and 0.1 M $Fe(NO_3)_3{\cdot}9H_2O$ were added to a mixture of 100 ml of 2-methoxyethanol and 15 ml of H_2O, followed by ultrasonication for 1 hr.

The multiferroic BTO/CFO nanocomposite was prepared by spin coating of BTO nanotube arrays with CFO precursor solution. The spin coating was carried out at 4000 rpm, and then the sample was pre-heated at 260 °C for 10 min. These processes were repeated 10 times to deposit a sufficient amount of CFO in the tubular pores of BTO. The sample was finally calcined at a heating rate of 5 °C min^{-1} and keeping a maximum temperature of 600 °C for 3 hrs.

The samples were observed with a scanning electron microscope (SEM, Acc. V: 15 kV, working distance: 8 mm, Hitachi S-4800, Japan) and a focused ion beam SEM (FIB-SEM, Acc. V: 40 kV for FIB and 3 kV for SEM, Hitachi NB-5000, Japan). Elemental distributions were analyzed by means of high angle annular dark field-scanning transmission electron microscopy-energy dispersive X-ray spectroscopy (HAADF-STEM-EDX, Acc. V: 200 kV, FEI Titan equipped with a Super-X EDX system, USA). The lamella used for HAADF-STEM-EDX analyses was prepared and cleaned using another FIB apparatus (Acc. V: 30 kV, FEI Helios Nanolab 450S, USA). An X-ray diffractometer (XRD, 40 kV, 20 mA, Rigaku Ultima IV, Japan) was used to analyze the crystal structure of the samples.

Piezoelectric simulations were performed using COMSOL Multiphysics, version 5.4. The geometry of the BTO/CFO nanocomposites was varied from multilayers to nanotube array-based nanocomposite. The electric potential at the bottom of the nanocomposites was set to be 5 V, while the top was grounded. Symmetry boundary conditions were employed for all sides of the model, and fixed constraint was applied to the bottom of the Ti substrate.

The magnetoelectric effect was evaluated by measuring the dielectric properties with a dielectric property evaluation system (Toyo Corporation, 6252Rev.C, Japan) under an external magnetic field applied with a Nd magnet (surface magnetic flux density: 3.5 kG) (see **Fig. S4** for a photo of the experimental setup). As for the dielectric property measurement, an Ag paste was applied on a ~1 mm^2 circled area of BTO/CFO nanocomposite to act as the upper electrode. A Ti substrate with a mechanically polished surface was used as the lower electrode.

The magnetic hysteresis loops of the samples were recorded with a vibrating sample magnetometer (VSM, step: 150 Oe, range: ±15 kOe, room temperature, a Ni sheet was used for calibration, Tamakawa, TM-VSM261483-HGC-SG, Japan). The pure CFO film was

prepared by 4-time spin coating of a Ti substrate with the CFO precursor solution.

Conclusions

We reported a novel nanotube array-based BTO-CFO nanocomposite film, which exhibits room temperature magnetoelectric multiferroics as well as perpendicular magnetic anisotropy. The film was fabricated solely via affordable liquid phase processes, which included anodization of a Ti sheet, hydrothermal treatment of TNTs in a $Ba(OH)_2$ containing aqueous solution, and spin coating of BTO NTs with a CFO precursor solution. The XRD and 3-D SEM analyses revealed that the nanocomposite film contained no undesired phase and that the volume fractions of BTO, CFO and void in the nanocomposite film were 78.6, 16.1 and 5.3 %, respectively. Even though the nanocomposite structure was not the same as the typical and often reported nanostructure, which is a dense nanopillar array-based one, it showed a room temperature magnetoelectric effect and weak perpendicular magnetic anisotropy. Importantly, the demonstrated novel liquid phase process provides a facile and affordable way to fabricate multifunctional multiferroic nanocomposite films.

Author contributions

G.K. designed the research. K.O. performed sample preparation, SEM observation, and VSM and magnetoelectric effect measurements. W.K.T. and X.W. assisted sample preparation. G.K., T.G. and N.Y. assisted VSM and magnetoelectric effect measurements. D.Y. performed 3-D SEM observation. F.L.D. and K.E.H. performed STEM-EDX observation. G.K., K.O., W.K.T., M.I., H.M., K.Y., A.R.B. and A.M. contributed to data discussion and to manuscript writing.

Conflicts of interest

There are no conflicts to declare.

Acknowledgements

This work was financially supported by the Program for Fostering Globally Talented Researchers (R2802), JSPS. TG, YN, and MI acknowledge JSPS KAKENHI [Grant Nos. 17K19029, 16H04329, and 26220902]. TG acknowledges JST PRESTO [Grant No. JPMJPR1524]. FLD acknowledges the N2020; Nanotechnology based functional solutions (NORTE-45-2015-02). The authors acknowledge the support of the Cooperative Research Facility Center at Toyohashi University of Technology.

References

1 W. Eerenstein, N. D. Mathur, J. F. Scott, *Nature* **2006**, *442*, 759.

2 C. Schmitz-Antoniak, D. Schmitz, P. Borisov, F. M. F. de Groot, S. Stienen, A. Warland, B. Krumme, R. Feyerherm, E. Dudzik, W. Kleemann, H. Wende, *Nature commun.* **2013**, *4*, 2051.

3 N. A. Spaldin, R. Ramesh, *Nature Mater.* **2019**, *18*, 203.

4 N. A. Hill, *J. Phys. Chem. B* **2000**, *104*, 6694.

5 A. M. J. G. Van Run, D. R. Terrell, J. H. Scholing, *J. Mater. Sci.* **1974**, *9*, 1710.

6 R. E. Newnham, S. Trolier-Mckinstry, *J. Appl. Cryst.* **1990**, *23*, 447.

7 J. Ryu, S. Priya, K. Uchino, H-E. Kim, *J. Electroceram.* **2002**, *8*, 107.

8 T-J. Lin, C-C. Chen, W. Lee, S. Cheng, Y-G. Chen, *Appl. Phys. Lett.* **2008**, *91*, 013108.

9 D. Viehland, J. F. Li, Y. Yang, T. Costanzo, A. Yourdkhani, G. Caruntu, P. Zhou, T. Zhang, T. Li, A. Gupta, M. Popov, G. Srinivasan, *J. Appl. Phys.* **2018**, *124*, 061101.

10 M. Buzzi, R. V. Chopdekar, J. L. Hockel, A. Bur, T. Wu, N. Pilet, P. Warniche, G. P. Carman, L. J. Heyderman, F. Nolting, *Phys. Rev. Lett.* **2013**, *111*, 027204.

11 M. Liu, X. Li, J. Lou, S. Zheng, K. Du, N. X. Sun, *J. Appl. Phys.* **2007**, *102*, 083911.

12 H-c. He, J. Ma, J. Wang, C-W. Nan, *J. Appl. Phys.* **2008**, *103*, 034103.

13 Y-D. Xu, G. Wu, H-L. Su, M. Shi, G-Y. Yu, L. Wang, *J. Alloys Compd.* **2011**, *509*, 3811.

14 S. H. Xie, Y. Y. Liu, J. Y. Li, *Front. Phys.* **2012**, *7*, 399.

15 Y. Shen, J. Sun, L. Li, Y. Yao, C. Zhou, R. Su, Y. Yang, *J. Mater. Chem. C* **2014**, *2*, 2545.

16 Y. Q. Liu, B. Zhang, Y. H. Wu, J. Zhang, D. Li, Y. Liu, M. B. Wei, J. H. Yang, *Superlattices Microstruct.* **2013**, *61*, 174.

17 D. Erdem, N. S. Bingham, F. J. Heiligtag, N. Pilet, P. Warnicke, C. A. F. Vaz, Y. Shi, M. Buzzi, J. L. M. Rupp, L. J. Heyderman, M. Niederberger, *ACS Nano* **2016**, *10*, 9840.

18 C. H. Jung, S. L. Woo, Y. S. Kim, K. S. No, *Thin Solid Films* **2011**, *519*, 3291.

19 H. Zheng, J. Wang, S. E. Lofland, Z. Ma, L. Mohaddes-Ardabili, T. Zhao, L. Salamanca-Riba, S. R. Shinde, S. B. Ogale, F. Bai, D. Viehland, Y. Jia, D. G. Schlom, M. Wuttig, A. Roytburd, R. Ramesh, *Science* **2004**, *303*, 661.

20 N. M. Aimon, H. K. Choi, X. Y. Sun, D. H. Kim, C. A. Ross, *Adv. Mater.* **2014**, *26*, 3063.

21 H. Kim, N. M. Aimon, X. Y. Sun, L. Kornblum, F. J. Walker, C. H. Ahn, C. A. Ross, *Adv. Funct. Mater.* **2014**, *24*, 5889.

22 N. M. Aimon, D. H. Kim, X. Y. Sun, C. A. Ross, *ACS Appl. Mater. Interf.* **2015**, *7*, 2263.

23 V. Tileli, M. Duchamp, A. K. Axelsson, M. Valant, R. E. Dunin-Borkowski, N. M. Alford, *Nanoscale* **2015**, *7*, 218.

24 G. Liu, C-W. Nan, Z. K. Xu, H. Chen, *J. Phys. D: Appl. Phys.* **2005**, *38*, 2321.

25 G. Kawamura, K. Ohara, W. K. Tan, T. Goto, Y. Nakamura, M. Inoue, H. Muto, K. Yamaguchi, A. R. Boccaccini, A. Matsuda, *Sci. Tech. Adv. Mater.* **2018**, *19*, 535.

26 G. Kawamura, K. Ohara, W. K. Tan, H. Muto, K. Yamaguchi, A. R. Boccaccini, A. Matsuda, *Mater. Lett.* **2018**, *227*, 120.

27 F. Zhang, S. Chen, Y. Yin, C. Xue, C. Lin, *Adv. Mater. Res.* **2009**, *79-82*, 617.
28 W. Liming, D. Xiangyun, L. Jianbao, L. Xinxing, Z. Guoqing, S. Kuifan, *J. Nanosci. Nanotechnol.* **2013**, *13*, 1.
29 G. Jian, D. X. Zhou, J. Y. Yang, H. Shao, F. Xue, Q. Y. Fu, *J. Eur. Ceram. Soc.* **2013**, *33*, 1155.
30 G. Sreenivasulu, M. Popov, F. A. Chavez, S. L. Hamilton, P. R. Lehto, G. Srinivasan, *Appl. Phys. Lett.* **2014**, *104*, 052901.
31 G. Sreenivasulu, M. Popov, R. Zhang, K. Sharma, C. Janes, A. Mukundan, G. Srinivasan, *Appl. Phys. Lett.* **2014**, *104*, 052910.
32 L. Zhou, Q. Fu, D. Zhou, Z. Zheng, Y. Hu, W. Luo, Y. Tian, C. Wang, F. Xue, X. Tang, *Appl. Phys. Lett.* **2017**, *111*, 032903.
33 V. Stancu, M. Lisca, I. Boerasu, L. Pintilie, M. Kosec, *Thin Solid Films* **2007**, *515*, 6557.
34 K. Mimura, K. Kato, *Appl. Phys. Express* **2014**, *7*, 061501.
35 Y. Podgorny, K. Vorotilov, P. Lavrov, A. Sigov, *Ferroelectrics* **2016**, *503*, 77.
36 J. H. Park, T-W. Lee, M. G. Kang, *Chem. Commun.* **2008**, 2867.
37 Y. C. Wang, J. Ding, J. B. Yi, B. H. Liu, T. Yu, Z. X. Shen, *Appl. Phys. Lett.* **2004**, *84*, 2596.
38 Y. Li, Z. Wang, J. Yao, T. Yang, Z. Wang, J-M. Hu, C. Chen, R. Sun, Z. Tian, J. Li, L-Q. Chen, D. Viehland, *Nature Commun.* **2015**, *6*, 6680.
39 S. E. Shirsath1, X. Liu, Y. Yasukawa, S. Li, A. Morisako, *Sci. Rep.* **2016**, *6*, 30074.
40 C. A. Ross, *Annu. Rev. Mater. Res.* **2001**, *31*, 203.
41 V. M. Prida, K. R. Pirota, D. Navas, A. Asenjo, M. Hernandez-Velez, M. Vazquez, *J. Nanosci. Nanotechnol.* **2007**, *7*, 272.

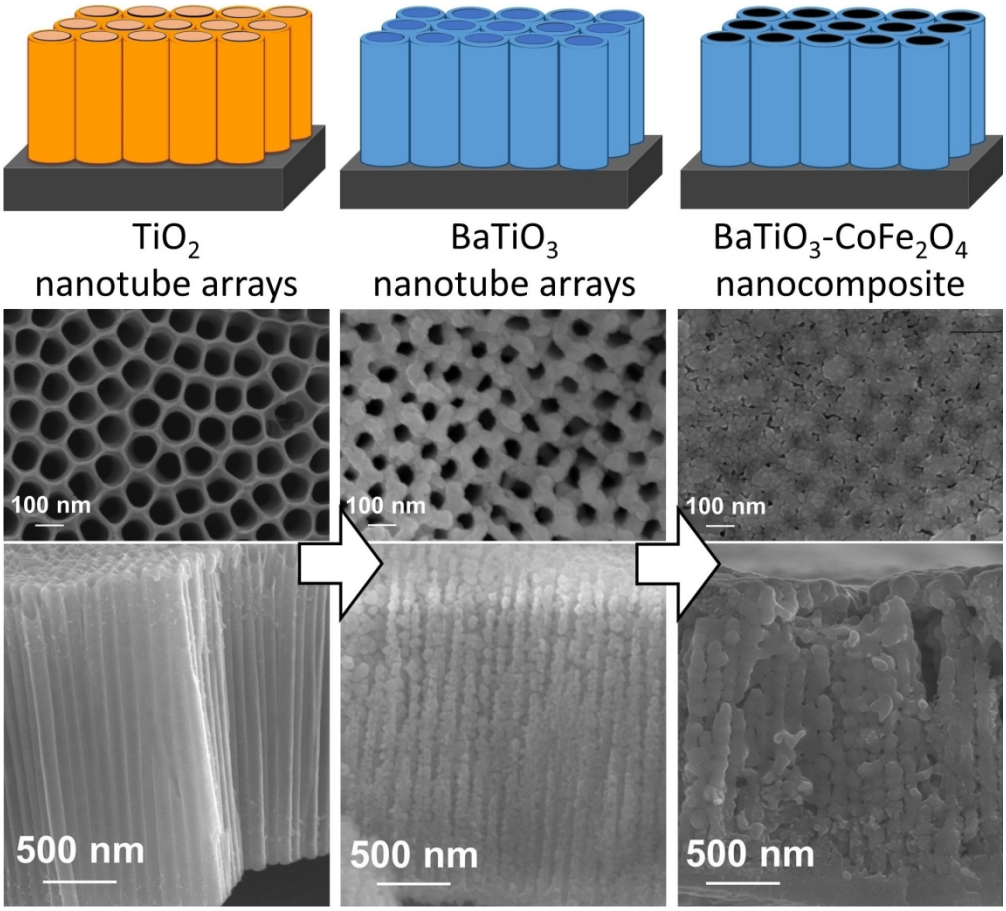

529x481mm (96 x 96 DPI)